RAA 2019 Vol. **19** No. **5**, 72(12pp) doi: 10.1088/1674–4527/19/5/72

http://www.raa-journal.org *http://iopscience.iop.org/raa*

***R**esearch in*
***A**stronomy and*
***A**strophysics*

The symmetry energy and incompressibility constrained by the observations of glitching pulsars

Yan Yan

School of Astronomy and Space Science, Nanjing University, Nanjing 210023, China; *2919ywhhxh@163.com*

Received 2018 May 19; accepted 2018 November 27

Abstract We investigate the masses of glitching pulsars in order to constrain their equation of state (EOS). The observations of glitches (sudden jumps in rotational frequency) may provide information on the interior physics of neutron stars. With the assumption that glitches are triggered by superfluid neutrons, the masses of glitching neutron stars can be estimated using observations of maximum glitches. Together with the observations of thermal emission from glitching pulsars Vela and J1709–4429, the slope of symmetry energy and incompressibility of nuclear matter at saturation density can be constrained. The slope of symmetry energy L should be larger than $67\,\mathrm{MeV}$ while the lower limit of incompressibility for symmetric nuclear matter K_0 is $215\,\mathrm{MeV}$. We also obtain a relationship between L and K_0: $6.173\,\mathrm{MeV} + 0.283K_0 \leq L \leq 7.729\,\mathrm{MeV} + 0.291K_0$. The restricted EOSs are consistent with the observations of 2-solar-mass neutron stars and gravitational waves from a binary neutron star inspiral.

Key words: neutron stars: glitch — neutron stars: cooling — neutron stars: tidal deformability — nuclear physics: symmetry energy

1 INTRODUCTION

Neutron stars, as remnants of supermassive stars, provide natural laboratories for isospin asymmetric nuclear matter at supra-saturation density. Many efforts have been made to constrain the equation of state (EOS) of cold, dense nuclear matter by both the observations of neutron stars and experiments in terrestrial laboratories.

During recent decades, significant progress has been achieved in development of the EOS of isospin asymmetric nuclear matter. Theoretical approaches have been used to predict common features of the EOS (Brueckner et al. 1968; Sjöberg 1974; Zuo et al. 2002; Brockmann & Machleidt 1984; Müther et al. 1987; Brockmann & Machleidt 1990; Sumiyoshi et al. 1992; Huber et al. 1994; Prakash et al. 1988; Gale et al. 1990; Chen et al. 2007). The symmetry energy and incompressibility at saturation density characterize the EOS of neutron stars. Terrestrial experimental data of the centroid energy of the giant dipole resonance for $^{208}\mathrm{Pb}$ (Trippa et al. 2008), isospin diffusion in heavy ion collisions (Tsang et al. 2009) and the energies of excitations due to isobaric analog states (Danielewicz & Lee 2014) provide information on the symmetry energy. By analyzing the observations of pulsars, Lattimer & Lim (2013); Lattimer (2012); Lattimer & Prakash (2016); Chen et al. (2009a); Pons et al. (2013); Hooker et al. (2015); Newton et al. (2014); Steiner et al. (2010); Steiner & Gandolfi (2012); Steiner et al. (2015) investigate the relation between the symmetry energy and observations of neutron stars. The ranges of constraints on both the terrestrial experiments and astrophysical observations are summarized in Lattimer & Prakash (2016); Newton et al. (2014). The constrained symmetry energy (E_{sym}) of the saturation density from the above experiments is around $31\,\mathrm{MeV}$. Moreover, the constraints on the slope of symmetry energy (L) at the saturation density give a range of $L \approx 58.7 \pm 28.1\,\mathrm{MeV}$ (Li 2004; Oertel et al. 2017). The incompressibility (K_0) of symmetric nuclear matter which determines the curvature of the EOS is also important. The value of incompressibility can be obtained from experimental data of isoscalar giant monopole and dipole resonances (compression modes) in nuclei (Brown & Osnes 1985; Shlomo et al. 2006).

Pulsar glitches (sudden jumps in rotational frequency) are traditionally thought to be a manifestation of vortex dynamics associated with a neutron superfluid (Anderson & Itoh 1975). Most studies of pulsars are based on a rigid model (Link et al. 1999; Andersson et al. 2012; Chamel 2013; Steiner et al. 2015; Newton et al. 2015; Ho et al. 2015). In this model, it is assumed that glitches are driven by superfluid neutrons in the inner crust. The average rate of angular momentum transfer indicates a minimum fraction of inertia that stores angular momentum (Link et al. 1999). If the entrainment is taken into account, the neutron superfluid in the neutron star crust does not carry enough angular momentum to explain the glitches (Chamel 2013; Andersson et al. 2012). The observations of glitches also offer a method to investigate the superfluid model (Ho et al. 2015). The discrepancy can also be solved by inducing crust-core coupling (Newton et al. 2015). Recently, Watanabe & Pethick (2017) announced that entrainment may be small if pairing is included in the calculation of effective masses in the crust. Moreover, Ho et al. (2015) estimate the masses of glitching pulsars cooperating with thermal observations. However, in their work, only S-wave pairing was taken into consideration. Pizzochero (2011); Antonelli & Pizzochero (2017) assume continuous vortex lines through the core (both S-wave and P-wave pairings). Under this assumption, Pizzochero et al. propose a new method to constrain the masses of glitching pulsars with their maximum glitches. In their study, among the 127 glitching pulsars, 16 objects can get both upper limits and lower limits of masses.

Neutron star cooling, which can provide information on superfluidity, has been extensively studied in recent decades (Yakovlev et al. 2001, 2002; Levenfish & Yakovlev 1996; Yakovlev et al. 1999). In these studies, three types of superfluidity are taken into consideration: singlet-state ($^1S_0$) superfluidity of neutrons and protons, and triplet-state ($^3P_2$) neutron superfluidity. The superfluidity of nucleons suppresses the neutrino process and affects nucleon heat capacities (Yakovlev et al. 1999). Moreover, the additional emission associated with Cooper pairing of nucleons appears (Flowers et al. 1976). Kaminker et al. (2002) attempt to analyze which critical temperatures are consistent with both the observations and microscopic calculations (Lombardo & Schulze 2001; Wambach et al. 1993; Schulze et al. 1996). From Yakovlev et al. (2002); Kaminker et al. (2002), we can figure out that the cooling behavior of medium-mass neutron stars is sensitive to both the superfluidity models and the EOS in the cores of neutron stars. They also provide a method to estimate the masses of neutron stars from their cooling behavior.

The aim of the present paper is to give a constraint on the slope of the symmetry energy and incompressibility from the observations. Many recent studies have focused on how symmetry energy influences the observations, such as the crust thicknesses, moments of inertia and tidal deformabilities (Hooker et al. 2015; Newton et al. 2015; Steiner et al. 2015). Instead of being concerned with the average rate of angular momentum transfer, we concentrate on the observations of maximum glitches. We assume a neutron star with $^1S_0$ neutron superfluid in the inner crust, and $^1S_0$ proton superfluid and $^3P_2$ neutron superfluid in the core. The vortex lines only pin to the inner crust. Thus we can evaluate the masses of glitching stars based on the work of Pizzochero et al. (2017). In conjunction with the predictions of masses from the observations of cooling of neutron stars, the EOS could be constrained. We also examine whether the restricted EOSs are consistent with the recent observation of GW170817.

In this paper, we combine the observations of maximum glitch and the cooling of neutron stars to constrain the EOS. The restricted EOSs are consistent with the observations of 2-solar-mass neutron stars and gravitational waves from a binary neutron star system.

This paper is organized as follows: the EOS is presented in Section 2 with the definitions of parameters. In Section 3, multiple observations are used to constrain the EOS. We also investigate whether the restricted EOSs are consistent with the constraints from GW170817 in the same section. A summary will be given in Section 4.

2 THE EQUATION OF STATE

The EOS of cold, dense nuclear matter is poorly understood. In this paper, we use an effective momentum dependent interaction (MDI) (Welke et al. 1988) which could be generalized to asymmetric nuclear matter (Das et al. 2003). In the core, the energy per nucleon of symmetric nuclear matter reads (Das et al. 2003; Chen et al. 2009b)

$$\begin{aligned} E_0(\rho) =& \frac{8\pi}{5mh^3\rho}p_f^5 + \frac{A_{\rm l}(x)+A_{\rm u}(x)}{4}\frac{\rho}{\rho_0} \\ &+ \frac{B}{\sigma+1}\frac{\rho^\sigma}{\rho_0^\sigma} + \frac{C_{\rm l}+C_{\rm u}}{3\rho\rho_0}\left(\frac{4\pi}{h^3}\right)^2\Lambda^2 \\ &\times\left[p_{\rm f}^2(6p_{\rm f}^2-\Lambda^2) - 8\Lambda p_{\rm f}^3\arctan\frac{2p_{\rm f}}{\Lambda}\right. \\ &\left.+\frac{1}{4}\left(\Lambda^4+12\Lambda^2p_{\rm f}^2\right)\ln\frac{4p_{\rm f}^2+\Lambda^2}{\Lambda^2}\right]. \end{aligned} \quad (1)$$

The symmetry energy can be obtained

$$
\begin{aligned}
E_{\rm sym}(\rho) &= \frac{1}{2}\Big(\frac{\partial^2 E}{\partial\delta^2}\Big)_{\delta=0} \\
&= \frac{8\pi}{9mh^3\rho}p_{\rm f}^5 + \frac{A_{\rm l}(x)-A_{\rm u}(x)}{4}\frac{\rho}{\rho_0} - \frac{Bx}{\sigma+1}\frac{\rho^\sigma}{\rho_0^\sigma} \\
&+ \frac{C_{\rm l}}{9\rho\rho_0}\Big(\frac{4\pi}{h^3}\Big)^2\Lambda^2\Big[4p_{\rm f}^4 - \Lambda^2 p_{\rm f}^2\ln\frac{4p_{\rm f}^2+\Lambda^2}{\Lambda^2}\Big] \\
&+ \frac{C_{\rm u}}{9\rho\rho_0}\Big(\frac{4\pi}{h^3}\Big)^2\Lambda^2\Big[4p_{\rm f}^4 - p_{\rm f}^2(4p_{\rm f}^2+\Lambda^2)\ln\frac{4p_{\rm f}^2+\Lambda^2}{\Lambda^2}\Big].
\end{aligned}
\tag{2}
$$

Here

$$
\begin{aligned}
&\rho = \rho_{\rm n}+\rho_{\rm p}, \quad \delta = \frac{\rho_{\rm n}-\rho_{\rm p}}{\rho}, \quad p_{\rm f} = \hbar\Big(3\pi^2\frac{\rho}{2}\Big)^{1/3}, \\
&\sigma = 4/3, \quad \Lambda = 1.0k_{\rm f}^0,
\end{aligned}
$$

where $k_{\rm f}^0$ is the Fermi momentum at the saturation density $0.16\ {\rm fm}^{-3}$. In Chen et al. (2005, 2009b), the parameters are chosen to be $A_{\rm l}(x)+A_{\rm u}(x) = -216.55\,{\rm MeV}$, $A_{\rm l}(x)-A_{\rm u}(x) = -24.59\,{\rm MeV}+4Bx/(\sigma+1)$, $B = 106.35\,{\rm MeV}$, $C_{\rm l} = -11.7\,{\rm MeV}$ and $C_{\rm u} = -103.4\,{\rm MeV}$. These parameters are obtained by fitting the momentum dependence of single-particle potential predicted by Gogny Hartree-Fock calculations. The parameter x is introduced to mimic the various theoretical predictions of momentum dependent symmetry energy (Chen et al. 2005). The other properties of the nuclear EOS at saturation density are fixed with various x.

From Figure 1, we can figure out that in the MDI(-1) and MDI(0) cases, the symmetry energy monotonically rises below $2\rho_0$, while in the MDI(1) case, the symmetry energy rises in the beginning and then begins to fall.

As mentioned in the introduction, the properties of the nuclear EOS vary with different theoretical approaches (Brueckner et al. 1968; Sjöberg 1974; Zuo et al. 2002; Brockmann & Machleidt 1984; Müther et al. 1987; Brockmann & Machleidt 1990; Sumiyoshi et al. 1992; Huber et al. 1994; Prakash et al. 1988; Gale et al. 1990; Chen et al. 2007). The values of incompressibility for nuclear matter predicted by various approaches give a large scatter (Li et al. 2008; Chen et al. 2009b). In order to produce continuous K_0 and L, we vary the parameters $A_{\rm l}(x)$, $A_{\rm u}(x)$, B, $C_{\rm l}$ and $C_{\rm u}$ to mimic different EOSs. For simplicity, we fix parameters $\sigma = 4/3$ and $\Lambda = 1.0k_{\rm f}^0$ to ensure a unique value for each parameter though this is not true for different interactions (Das et al. 2003). The predictions of basic properties of asymmetric nuclear matter with the different sets of parameters should be consistent with the observations in terrestrial laboratories and the constraints from pulsars.

The critical properties at saturation density of nuclear matter are:

$$
\begin{aligned}
&\rho_0 = 0.16\ {\rm fm}^{-3}, \ \ E_0 = -16\ {\rm MeV}, \\
&K_0 = (220\pm20)\ {\rm MeV}, \ \ E_{\rm sym} = 31\ {\rm MeV}, \\
&L = (60\pm20)\ {\rm MeV}, \ \ m_{\rm Landau}/m_{\rm n} \le 1\ ,
\end{aligned}
\tag{3}
$$

where $K_0 = 9\rho_0^2\frac{\partial^2 E_0(\rho)}{\partial\rho^2}|_{\rho=\rho_0}$ is the incompressibility of symmetric nuclear matter and $L = 3\rho_0\frac{\partial E_{\rm sym}(\rho)}{\partial\rho}|_{\rho=\rho_0}$ is the slope of symmetry energy. $m_{\rm Landau} = k(dk/d\epsilon_k)|_{k=k_{\rm f}}$ is defined to be the Landau mass, where ϵ_k is the nucleon single-particle energy (Jeukenne et al. 1976; Negele & Yazaki 1981). The range of parameter L is consistent with the experimental constraints discussed in Lattimer & Prakash (2016). The range of incompressibility of the symmetric nuclear matter is given from giant monopole resonances (Blaizot 1980; Shlomo et al. 2006). Moreover, the Landau mass is widely discussed in both nuclear physics and astrophysics (especially for neutron stars and supernovae) (Cooperstein 1985; Jeukenne et al. 1976; Negele & Yazaki 1981; Farine et al. 2001). Jeukenne et al. (1976); Negele & Yazaki (1981); Farine et al. (2001) discuss the issue that $m_{\rm Landau}/m_{\rm n}$ should be less than 1. However, for some parameters, $m_{\rm Landau}/m_{\rm n}$ will exceed 1 as exhibited in Figure 2. We exclude those parameters to ensure $m_{\rm Landau}/m_{\rm n}$ is below 1. We choose $m_{\rm n} = 939\,{\rm MeV}$ in this work.

3 THE OBSERVATIONS OF NEUTRON STARS

3.1 Mass-radius Relation of Neutron Stars

The observations of masses and radii of neutron stars can be used to constrain the EOS. Due to the lack of precise measurements of radii, the constraints are really weak. The observations of J1614–2230 (Demorest et al. 2010) and J0348+0432 (Antoniadis et al. 2013) yield 2-solar-mass neutron stars. These observations can place lower bounds on the stiffness of the EOS.

In neutron stars, β-equilibrium and a charge neutral condition should be taken into consideration. For npe matter, one has

$$\mu_{\rm n} - \mu_{\rm p} = \mu_{\rm e}, \tag{4}$$

$$\rho_{\rm p} = \rho_{\rm e}, \tag{5}$$

where $\mu_{\rm n}$, $\mu_{\rm p}$ and $\mu_{\rm e}$ denote the chemical potential of the neutron, proton and electron respectively. The parabolic approximation of the EOS is used here

$$\mu_{\rm e} \approx 4(1-2x_{\rm p})E_{\rm sym}, \tag{6}$$

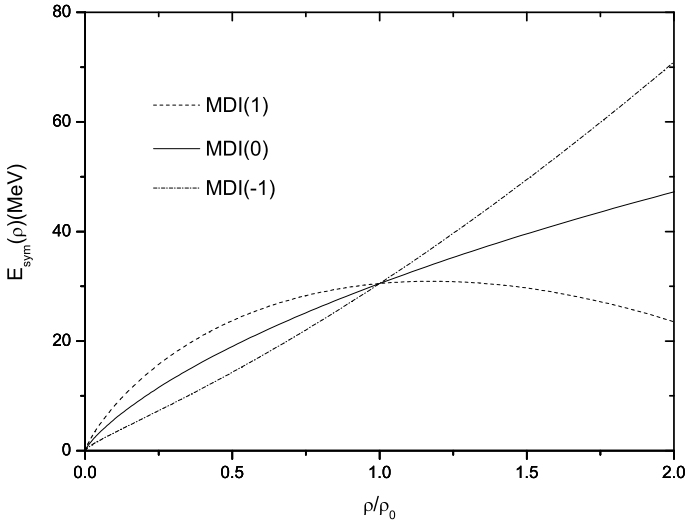

Fig. 1 The symmetry energy of MDI(1), MDI(0) and MDI(-1).

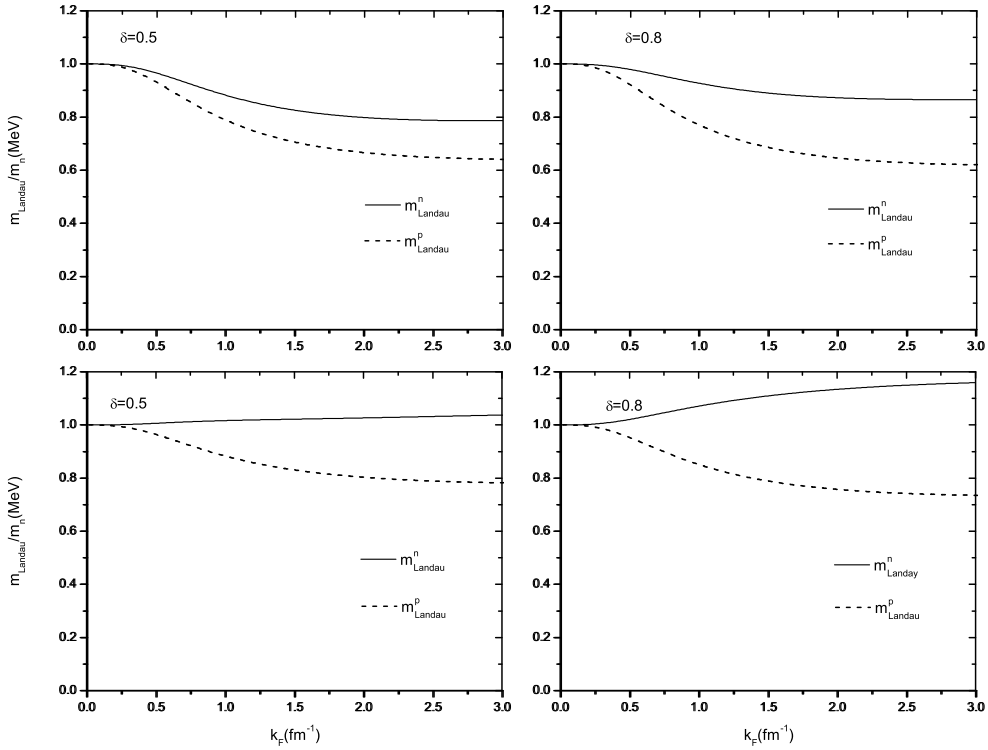

Fig. 2 $m^n_{\rm Landau}$ and $m^p_{\rm Landau}$ denote the neutron and proton Landau mass, respectively. The Landau masses for neutrons and protons in the different panels have different parameters. The upper panels display the Landau mass with parameters $K_0 = 213$ MeV and $L = 61$ MeV . The lower panels feature the Landau mass with parameters $K_0 = 230$ MeV and $L = 60$ MeV.

where $x_{\rm p} = \frac{1-\delta}{2}$ is the fraction of protons. With the calculations of Equations (1) and (2), the EOS can be obtained

$$\epsilon_{\rm total}(\rho,\delta) = \rho[E_0(\rho) + E_{\rm sym}\delta^2] + \rho m + \epsilon_{\rm e}(\rho,\delta), \quad (7)$$

$$P_{\rm total}(\rho,\delta) = \rho^2(E_0'(\rho) + E_{\rm sym}'(\rho)\delta^2) + P_{\rm e}(\rho,\delta), \quad (8)$$

where $\delta = (1-2x_{\rm p})$, and $\epsilon_{\rm total}$ and $P_{\rm total}$ denote the total density energy and the total pressure respectively. $\epsilon_{\rm e}(\rho,\delta)$ and $P_{\rm e}(\rho,\delta)$ can be calculated using a non-interacting Fermi gas model. m and ρ denote baryon mass and total baryon density respectively. Chen et al. (2009b) pointed out that this model cannot be applied in the low pressure region due to instability. When we refer to neutron stars, the Skyrme force (Douchin & Haensel 2001) is introduced to describe the crust.

In order to obtain the mass-radius relations for non-rotating neutron stars, we substitute $\epsilon_{\rm total}$ and $P_{\rm total}$ into

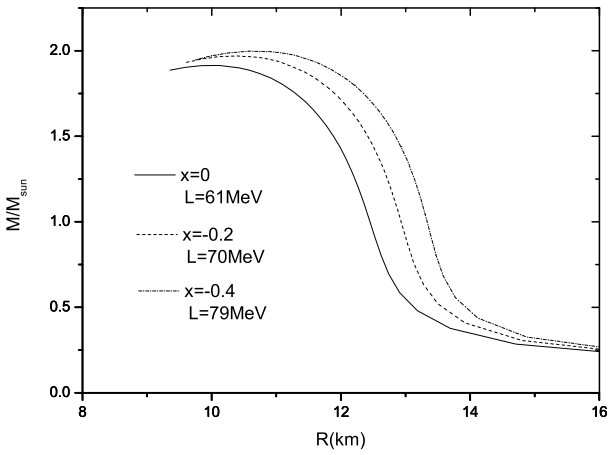

Fig. 3 The mass-radius relations for MDI(0), MDI(-0.2) and MDI(-0.4). K_0 is fixed at 213 MeV.

the Tolman-Oppenheimer-Volkoff equation

$$\frac{dP(r)}{dr} = -\frac{G(\varepsilon + P)(M + 4\pi r^3 P)}{r(r - 2GM)}, \quad (9)$$

$$\frac{dM(r)}{dr} = 4\pi r^2 \varepsilon. \quad (10)$$

In Figure 3, we plot the mass-radius relations of $x = 0$, $x = -0.2$ and $x = -0.4$ with the parameters in Chen et al. (2005, 2009b). The corresponding values of L are 61 MeV, 70 MeV and 79 MeV. The maximum mass of MDI(0) is $1.92\,M_\odot$ which is incompatible with 2-solar-mass observations (Demorest et al. 2010; Antoniadis et al. 2013). When $x \leq -0.2$, the maximum mass exceeds $1.97\,M_\odot$. Since a change of x keeps the same incompressibility, only the symmetry energy is responsible for the differences in mass-radius relations in Figure 3. The maximum masses of different x vary slightly while the radii change obviously. The same conclusion was made by Li et al. (2008) that the radius is more sensitive to symmetry energy than maximum mass.

Moreover, we examine the parameter space of K_0 and L when x is fixed to be 0. From Figure 4, we deduce that the larger values of K_0 and L lead to stiffer EOSs which are compatible with 2-solar-mass observations (Demorest et al. 2010; Antoniadis et al. 2013). It can be found that the allowed parameters are exhibited by the solid line of $1.97\,M_\odot$ and the dash-dotted line signifies the correct Landau mass. Small values of L which may lead to negative pressure are fully excluded. The minimum L is about 64 MeV. We also examine the ranges of parameters with different σ which varies in different interactions. The allowed parameters are changed. For $\sigma = 3/2$, the minimum allowed L is below 56 MeV. However, in the following work, we discuss the case of $\sigma = 4/3$ as an example.

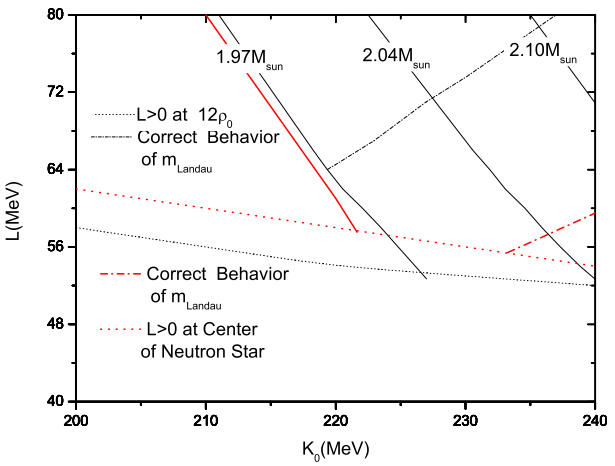

Fig. 4 The range of parameters K_0 and L when x is fixed to be 0. The parameters under the *dotted line* are not suitable for describing neutron stars because of the small or negative L (Rikovska Stone et al. 2003) which may lead to negative pressure that is forbidden physically. Here we should notice that the central densities of the neutron stars with maximum masses are around $7-8\rho_0$. We choose $L \geq 0$ MeV at $12\rho_0$ to ensure the pressure can be calculated. This constraint is conservative. The *solid lines* signify the contours representing maximum masses of $1.97\,M_\odot$, $2.04\,M_\odot$ and $2.10\,M_\odot$. The parameters under the *dash-dotted line* would produce $m^n_{\rm Landau}/m_{\rm n}$ which exceeds 1. The *gray lines* give a range of allowed parameter space with $\sigma = 3/2$ mentioned in Eq. (1) and Eq. (2). *Color online.*

3.2 Maximum Glitches in Neutron Stars

A glitch in a neutron star is believed to offer a unique glimpse into its interior physics. Many studies have been concerned with the average rate of angular momentum transfer. Observations of glitches can give a lower limit for the crustal fraction of the moment of inertia ratio ($\Delta I/I = 0.14$) (Link et al. 1999). Some researches related to the EOS also treat this as a strong constraint (Chen et al. 2009b; Li et al. 2008). When the entrainment is taken into account, the moment of inertia associated with the angular momentum reservoir is severely reduced (Andersson et al. 2012; Chamel 2013). The conflict between observation of a glitch and the associated theory inspired the study of crust-core coupling (Newton et al. 2015). In Ho et al. (2015), only the SFB model out of nine superfluid models can account for observations of the Vela glitch. Moreover, the masses of glitching neutron stars are estimated. In their work, only a neutron superfluid in the singlet-state is considered. In the core of a neutron star, neutrons may be in a superfluid triple-state ($^3P_2$). The rapid cooling of Cassiopeia A is treated as evidence for the existence of $^3P_2$ (Page et al. 2011; Shternin et al. 2011). In our work, we adopt continuous vortex lines through the core of a neutron star neglecting the interface of $^1S_0$ and $^3P_2$ (Antonelli

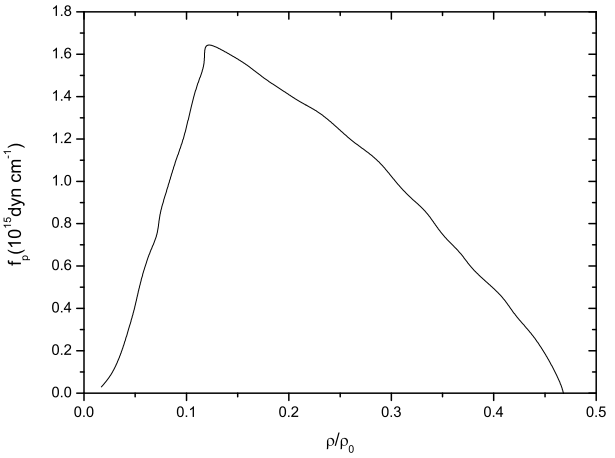

Fig. 5 The pinning force profile per unit length. The pinning force is zero out of the density range $0.0016\rho_0 \leq \rho \leq 0.47\rho_0$, where $\rho_0 = 0.16\,\mathrm{fm}^{-3}$.

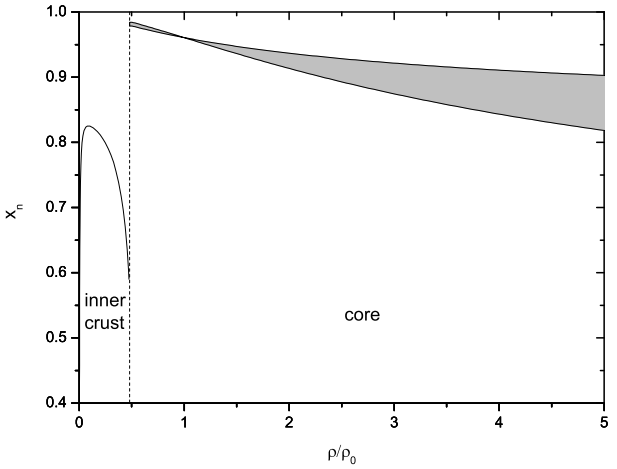

Fig. 6 The neutron fraction x_n. The *solid line* is the neutron fraction of the inner crust. The *gray region* is the range of neutron fraction in the core with different K_0 and L permitted by 2-solar-mass observations and basic nuclear physics discussed in the previous section. The *dashed line* is the crust-core interface at $0.47\rho_0$.

& Pizzochero 2017; Pizzochero et al. 2017). The reduction to a rigid model was discussed in Antonelli & Pizzochero (2017). A large reservoir of angular momentum which can account for the glitch of Vela is obtained. Based on Antonelli & Pizzochero (2017), Pizzochero et al. (2017) proposed a new method to measure the masses of glitching pulsars. Instead of considering the average rate of angular momentum transfer, the maximum glitch was studied.

The maximum lag between superfluid neutrons and normal matter can be calculated by balancing the pinning force and the Magnus force

$$\omega_\mathrm{cr}(x) = \frac{F_\mathrm{P}(x)}{\kappa x b(x)}\ , \tag{11}$$

where $\kappa = \pi\hbar/m_\mathrm{n}$ is the quantum of circulation. The total pinning force can be calculated by integrating the pinning per unit length $f_\mathrm{P}(x)$ which is plotted in Figure 5 (Seveso et al. 2016) along the straight vortex lines

$$F_\mathrm{P} = 2\int_0^{z(x)} f_\mathrm{P}(r)dz\ , \tag{12}$$

$$b(x) = 2\int_0^{z(x)} dz\frac{\rho_\mathrm{n}(r)}{1-\epsilon_\mathrm{n}(r)}\ , \tag{13}$$

where $\rho_\mathrm{n}(r) = x_\mathrm{n}(r)\rho(r)$ and $z(x) = \sqrt{R^2-x^2}$, and x is the distance from the rotational axis. (It is different from the x in Section 2.) $x_\mathrm{n}(r)$ plotted in Figure 6 is the superfluid neutron fraction and $\epsilon_\mathrm{n}(r)$ is the entrainment. Entrainment should be included in the multi-fluid problem. We use the studies of superfluid entrainment by Chamel for the crust (Chamel 2012) and the core (Chamel & Haensel 2006). We utilize the definition of effective mass m_n^* in Chamel & Haensel (2006) to parameterize the entrainment with the form $\epsilon_\mathrm{n} = 1 - m_\mathrm{n}^*/m_\mathrm{n}$. The range of effective masses is plotted in Figure 7 with the different parameters describing the core. We infer that the parameters make little difference to the entrainment in the core. The range of $m_\mathrm{n}^*/m_\mathrm{n}$ is from $0.96 \sim 0.99$. The most important part of the entrainment is in the inner crust derived from Chamel (2012). The above calculations assume parallel straight vortex lines pinned only to the inner crust. According to angular momentum conservation, the maximum permitted glitch can be obtained.

$$\Delta\Omega_\mathrm{max} = \frac{I_\nu}{I}\left\langle\omega_\mathrm{cr}(x)\right\rangle\ . \tag{14}$$

$$I_\nu = \frac{8\pi}{3}\int_0^R drr^4\frac{\rho_\mathrm{n}(r)}{1-\epsilon_\mathrm{n}(r)}, \tag{15}$$

$$I = \frac{8\pi}{3}\int_0^R drr^4\rho(r). \tag{16}$$

I_ν and I denote the moment of inertia of component n and the total moment of inertia in the Newtonian approximation respectively. Both I_ν and ω_cr are related to the entrainment. They finally cancel out analytically during the calculation of maximum glitch.

As mentioned in Pizzochero et al. (2017), there is a general inverse correlation between the size of the maximum glitch and the pulsar mass. Figures 8 and 9 illustrate that larger values of L and K_0 lead to larger maximum permitted glitches, and thus larger upper limits of masses for glitching neutron stars. This upper limit is robust. For different x in the MDI model, L changes when

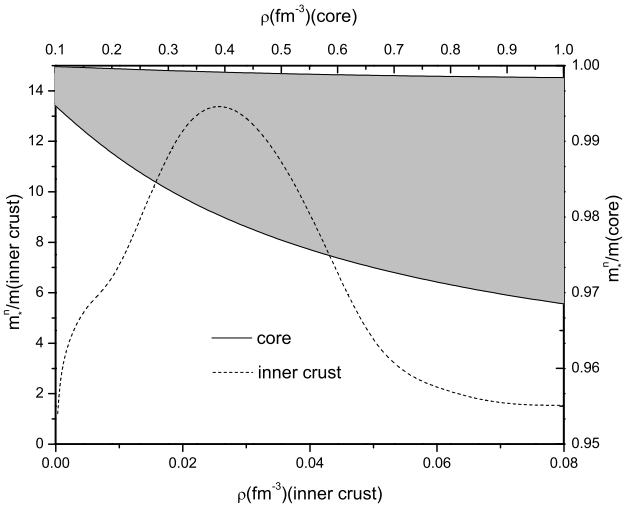

Fig. 7 The entrainment $\epsilon_{\rm n}$. The *dashed line* is the entrainment of the inner crust. The *gray region* is the range of entrainment in the core with different K_0 and L permitted by 2-solar-mass observations and basic nuclear physics discussed in the previous section.

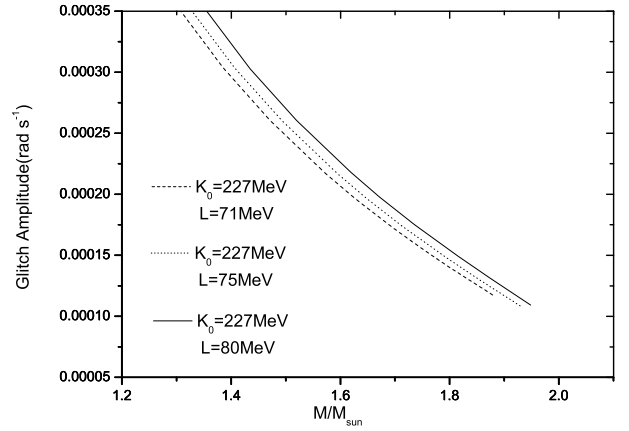

Fig. 8 Upper limits of the masses for glitching pulsars with different L.

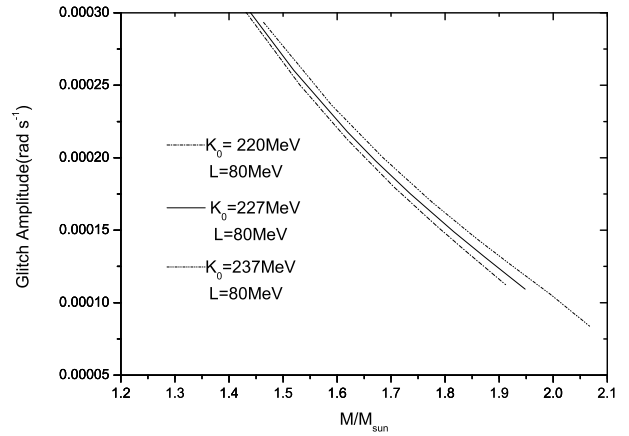

Fig. 9 Upper limits of the masses for glitching pulsars with different K_0.

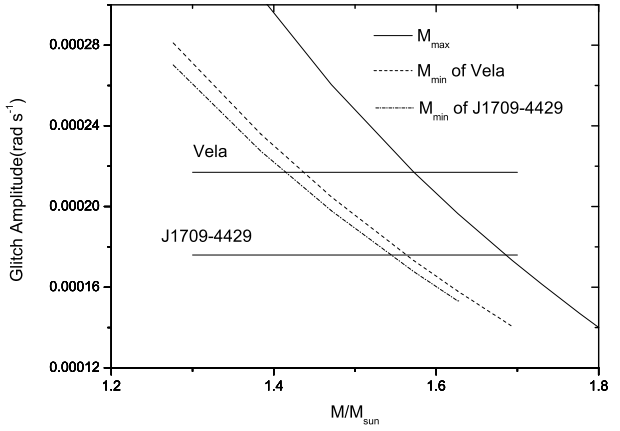

Fig. 10 The mass ranges of J1709–4429 and Vela. For the parameters of the EOS, K_0 and L assume the values 227 MeV and 71 MeV respectively with $x = 0$. The observation data of J1709–4429 and Vela are listed in table 1 in Pizzochero et al. (2017).

the incompressibility is fixed. The trend is similar to what is displayed in Figure 8.

An additional assumption should be added if we want to calculate the lower limit of the mass of a glitching neutron star. Pizzochero et al. (2017) assume that the maximum glitch depletes the whole available reservoir of angular momentum stored since co-rotation. This will give a minimum mass for a glitching neutron star. The nominal lag $\omega^*_{\rm pre}$ can be obtained

$$\omega^*_{\rm pre} = t_{\rm pre} \times |\dot{\Omega}| \tag{17}$$

where $t_{\rm pre}$ represents the waiting time between the maximum observed glitch and the previous one, and $|\dot{\Omega}|$ is the spin-down rate.

In this partial filling situation, the accumulated lag reads

$$\omega_{\rm t}(x) = \min[\omega_{\rm cr}(x), \omega^*_{\rm pre}] \ . \tag{18}$$

From this reservoir, we can derive the angular momentum which is depleted during a glitch. According to conservation of angular momentum

$$\Delta\Omega_{\rm t} = \frac{I_\nu}{I} \left\langle \omega_{\rm t}(x) \right\rangle \ . \tag{19}$$

This result is obviously related to the entrainment. Due to the similarity between Equation (14) and Equation (19), changes in the trend with K_0 or L are the same.

Once the microphysical input is fixed, the range of mass for a glitching star can be obtained by calculating Equation (14) and Equation (19).

Figure 10 shows the different ranges for J1709–4429 and Vela. If the nominal lag is large, the constraint on the mass of the glitching pulsar will be tighter. Although

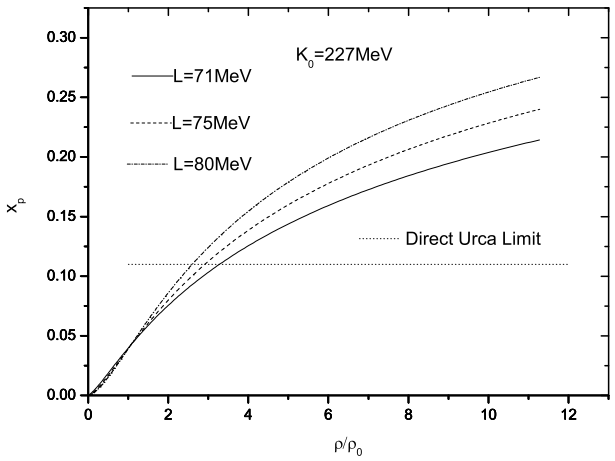

Fig. 11 The proton fraction with different L. The *dotted line* is the direct Urca threshold.

we can obtain the different masses of 17 objects listed in Pizzochero et al. (2017) with various parameters, there is no mass measurement for a glitching neutron star. The slope of symmetry and incompressibility of the EOS cannot be constrained only by the observations of maximum glitches.

3.3 Thermal Observations

The cooling of neutron stars depends on the properties of dense matter. Since the last century, several candidates for thermally-emitting neutron stars have been discovered (Pavlov et al. 2002). Neutrino cooling dominates for at least the first thousand years after its birth. Photon emission eventually exceeds neutrino emission when the internal temperature has sufficiently dropped. Many theoretical studies have simulated neutron star cooling with fully relativistic non-isothermal cooling code (Gnedin et al. 2001; Yakovlev et al. 2001, 2002; Levenfish & Yakovlev 1996; Yakovlev et al. 1999; Kaminker et al. 2002). In the absence of hyperons and quarks, the dominant neutrino processes are modified and direct Urca processes and bremsstrahlung processes appear. The emissivity of direct Urca is more efficient than that of modified Urca. For a neutron star made of protons, neutrons and electrons, the critical proton fraction of the direct Urca threshold is about 11%.

From Figure 11, the critical density ($\rho_{\rm D}$) when the direct Urca process appears decreases with larger L. It is similar for different x in the MDI model. The smaller x indicates earlier occurrence of direct Urca. We deduce that the proton fraction is closely related to the symmetry energy while being almost independent of incompressibility K_0 according to Equation (6). In non-superfluid neutron stars, a sharp transition from slow (modified Urca) to fast (direct Urca) cooling takes place.

In Kaminker et al. (2002), the cooling of middle-aged neutron stars can be divided into three types: (I) slowly cooling NSs where the direct Urca process is forbidden or strongly suppressed by the superfluid protons; (II) moderately cooling NSs where the direct Urca process is suppressed by the superfluid protons; and (III) fast cooling NSs where the direct Urca process is weakly suppressed by the superfluid protons. Both slowly cooling NSs and fast cooling NSs are not sensitive to the EOS. However, Vela and J1709–4429 can be attributed to the moderately cooling stars which are intimately related to the EOS. The authors of Kaminker et al. (2002) obtained simple estimates of the mass ranges for moderately cooling stars. $M_{\rm I}$ is the mass when $T_{\rm cp}(\rho_{\rm c}) = T^I_{\rm cp}(\rho_{\rm c})$, where $T_{\rm cp}(\rho_{\rm c})$ is the critical temperature of superfluid protons in the center of a neutron star. A simple estimation of $T^I_{\rm cp}(\rho_{\rm c})$ is $5.5T$ for $\rho \leq \rho_{\rm D}$, and $17T$ for $\rho \geq \rho_{\rm D}$. Similarly, $M_{\rm II}$ is the mass when $T_{\rm cp}(\rho_{\rm c}) = T^{II}_{\rm cp}(\rho_{\rm c})$, where $T^{II}_{\rm cp}(\rho_{\rm c})$ is $3T$. T is the internal temperature of a neutron star. We choose $T_{\rm Vela}$ equal to 1.2×10^8 K and $T_{J1709-4429}$ equal to 0.7×10^8 K (Ho et al. 2015). The mass of a moderately cooling star satisfies the relation $M_{\rm I} \leq M \leq M_{\rm II}$. We use these ranges to characterize the masses of Vela and J1709–4429 from cooling observations.

In this work, we apply the parametrization of the critical temperature of proton superfluid (1p)

$$T_{\rm cp} = T_0 \frac{(k_{\rm fp}-k_0)^2}{(k_{\rm fp}-k_0)^2+k_1^2}\frac{(k_{\rm fp}-k_2)^2}{(k_{\rm fp}-k_2)^2+k_3^2}$$

for $k_0 < k_{\rm p} < k2$; and $T_{\rm c} = 0$ for $k_{\rm p} \leq k_0$ or $k_{\rm p} \geq k_2$, where $T_0 = 2.029\times10^{10}$ K, $k_0 = 0\,{\rm fm}^{-1}$, $k_1 = 1.117\,{\rm fm}^{-1}$, $k_2 = 1.241\,{\rm fm}^{-1}$ and $k_3 = 0.1473\,{\rm fm}^{-1}$ in the 1p model, and $T_0 = 1.7\times10^{10}$ K, $k_0 = 0\,{\rm fm}^{-1}$, $k_1 = 1.117\,{\rm fm}^{-1}$, $k_2 = 1.329\ {\rm fm}^{-1}$ and $k_3 = 0.1179\,{\rm fm}^{-1}$ in the 2p model. $k_{\rm fp}$ can be determined from the density and proton fraction according to $k_{\rm fp} = \hbar(3\pi^2 x_{\rm p}\rho)^{1/3}$.

The ranges of masses evaluated from both the maximum glitch and cooling with the 1p and 2p models are displayed in Figures 12 and 13. The parameter sets satisfy the 2-solar-mass observations and basic nuclear properties. Some common properties can be deduced: (I) The critical mass of direct Urca ($M_{\rm D}$) decreases with increasing L. This can be explained as the early onset of direct Urca with large L. (II) The values of $M_{\rm I}$ and $M_{\rm II}$ decrease with increasing L. This is because the value of $k_{\rm fp}$ of the critical temperature is fixed. According to $k_{\rm fp} = \hbar(3\pi^2 x_{\rm p}\rho)^{1/3}$, ρ will be smaller for larger L due to the larger $x_{\rm p}$. Though the larger L will lead to a stiffer EOS, the effect can

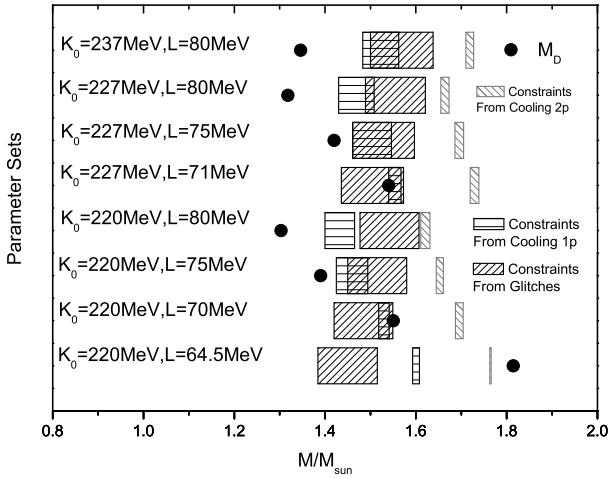

Fig. 12 The masses of Vela evaluated from maximum glitch and cooling with different parameters.

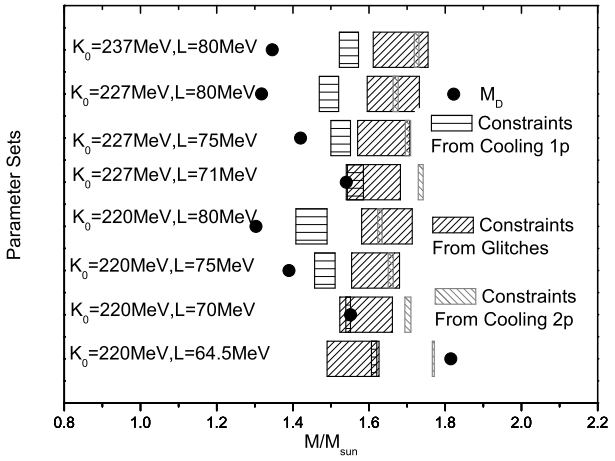

Fig. 13 The masses of J1709–4429 evaluated from maximum glitch and cooling with different parameters.

be neglected. (III) As mentioned in the previous section, the ranges of masses obtained from maximum glitches increase with L. The inverse relationships (II) and (III) ensure the constraint of the EOS. From Figure 12, for the 1p model with the parameters $K_0 = 220\,\mathrm{MeV}$, $L = 64.5\,\mathrm{MeV}$ and $K_0 = 220\,\mathrm{MeV}$, $L = 80\,\mathrm{MeV}$, the masses obtained by the maximum glitch and cooling behavior cannot overlap. That means that for Vela, the masses predicted by the maximum glitch and by cooling are different. When the superfluid model is fixed, only the EOS is responsible for this discrepancy. The two sets of parameters should be excluded. For the fixed incompressibility $K_0 = 220\,\mathrm{MeV}$, the slope of symmetry energy has both an upper limit and a lower limit. For J1709–4429, the lower limit L disappears but the upper limit is lower. For a special K_0, the lowest L is determined by $\max[M_{\mathrm{Glitch}}] = M_{\mathrm{I}}$ for Vela while the highest L is determined by $\min[M_{\mathrm{Glitch}}] = M_{\mathrm{II}}$

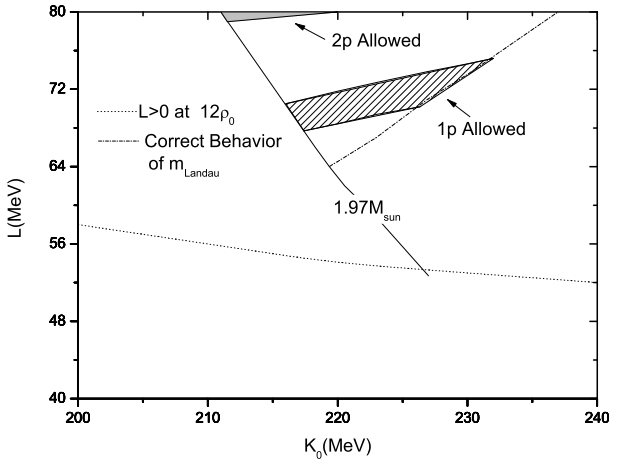

Fig. 14 The restricted parameters are in the shaded regions.

for J1709–4429, and M_{Glitch} is the range of masses obtained in Section 3.2. For the 2p model, both Vela and J1709–4429 give the lower boundary of L for fixed K_0. The minimum L is 79 MeV, which will be excluded by the observation of GW170817 in the next section. The parameters constrained by the method are shown in Figure 14. It can be deduced that the lower limits of K_0 and L correspond to $215\,\mathrm{MeV}$ and $67\,\mathrm{MeV}$ respectively in the 1p model. Moreover, we can find the relationship between K_0 and L for the 1p model: $6.173\,\mathrm{MeV} + 0.283K_0 \leq L \leq 7.729\,\mathrm{MeV} + 0.291K_0$. We also examine the EOS of MDI(-0.2) with the parameters derived from the Gogny interaction (Chen et al. 2005, 2009b). The ranges of masses predicted by maximum glitch and cooling of J1709–4429 are $1.530 - 1.663\,M_\odot$ and $1.451 - 1.495\,M_\odot$ respectively in the 1p model. MDI(-0.2) will be ruled out due to the inconsistency of the masses. As was stated in Section 3.1, $x \leq -0.2$ ensures a consistent result with 2-solar-mass observations. However, with smaller x, the mass predicted by the cooling of J1709–4429 will be smaller while that predicted by the maximum glitch will be larger. Therefore, the MDI EOS based on the Hartree-Fock calculation using the Gogny interaction is excluded.

Moreover, the masses of Vela and J1709–4429 can also be restricted to narrow ranges due to overlap of the two constraints. The masses of Vela and J1709–4429 are $1.45\,M_\odot \sim 1.55\,M_\odot$ and $1.53\,M_\odot \sim 1.62\,M_\odot$ respectively. The constrained masses are generally smaller than those predicted in Ho et al. (2015). It is easy to comprehend that Ho et al. (2015) assume only the inner crust accounts for the glitch. In this case the neutron star should be more massive to store enough angular momentum. The direct measurements of glitching pulsars may help us to judge which sections participate during the glitch.

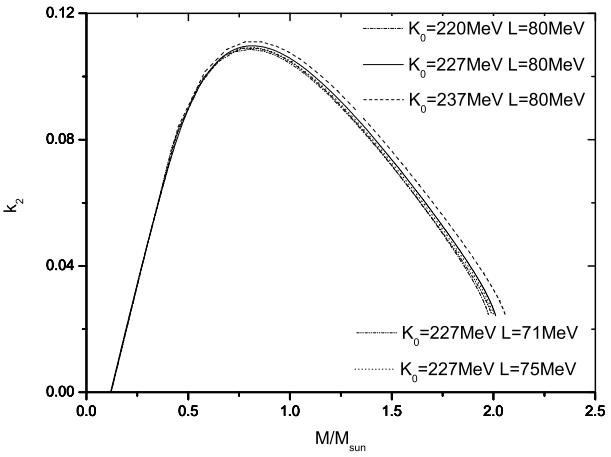

Fig. 15 The ranges of k_2 with different parameters.

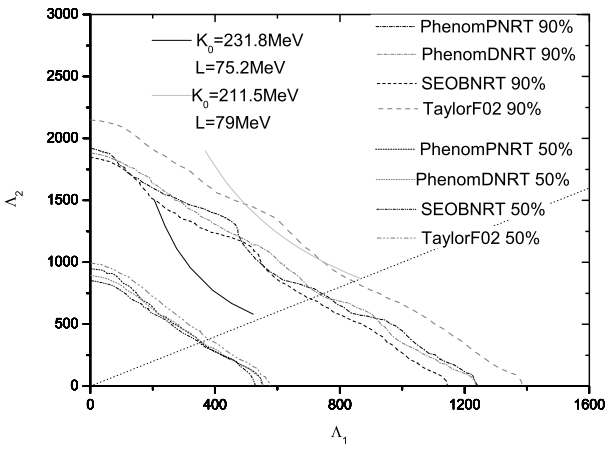

Fig. 16 The ranges of Λ_1 and Λ_2 for the higher limit with $x = 0$. Λ_1 and Λ_2 denote the dimensionless tidal deformability parameters of m_1 and m_2 respectively. The *dotted line* indicates the $\Lambda_1 = \Lambda_2$ boundary. The *dashed lines* signify the 90% and 50% contours constrained for the observation of GW170817 with the low-spin prior. The parameters of the upper limit are $K_0 = 231.8\,\mathrm{MeV},\ L = 75.2\,\mathrm{MeV}$ for the 1p model, while those of the lower limit are $K_0 = 211.5\,\mathrm{MeV},\ L = 79\,\mathrm{MeV}$ for the 2p model.

3.4 Tidal Deformability Constrained by GW170817

On 2017 August 17, the Advanced LIGO and Virgo network detected a gravitational-wave signal from a binary neutron star merger. During the late inspiral, the phase evolution of gravitational waves will be affected by tidal effects, which is related to the EOS (Hinderer et al. 2010). The tidal deformability allowed by the event GW170817 gives another constraint on the EOS. The tidal deformability parameter λ describes the ratio of each star's induced quadrupole to the tidal field of its companion. It is related to a dimensionless quantity k_2, called the Love number: $\lambda = 2/(3G)k_2R^5$. With the restricted EOS, we can calculate k_2.

From Figure 15, we can figure out that larger values of K_0 and L lead to larger k_2. In order to compare with the observation of GW170817, Figure 16 shows the predictions of the higher limit with $x = 0$ that we can obtain in this work together with the 90% and 50% probabilities of the observation constraint (The LIGO Scientific Collaboration et al. 2018). We can figure out that the prediction of the restricted EOS (1p model) is inside the 90% probability region for the low-spin prior, while the lower limit of the 2p model is excluded by GW170817.

With the leading order for Λ_1 and Λ_2, the weighted average $\widetilde{\Lambda}$ can be obtained

$$\widetilde{\Lambda} = \frac{16}{13}\frac{(m_1 + 12m_2)m_1^4\Lambda_1 + (m_2 + 12m_1)m_2^4\Lambda_2}{(m_1 + m_2)^5}. \tag{20}$$

In the low-spin case, $\widetilde{\Lambda} \leq 800$ with 90% probability. For the EOSs allowed in the previous sections, $\widetilde{\Lambda} \leq 603$. This result is consistent with the observation.

Moreover, the associated electromagnetic emission of GW170817 suggests that the merger did not result in a prompt collapse (Kasen et al. 2017; Metzger 2017). In Bauswein et al. (2017), the radius of a neutron star can be constrained if the merging neutron stars can result in an at least transiently stable neutron star. They put lower limits of $10.68^{+0.15}_{-0.04}$ km on non-rotating neutron stars with a mass of $1.6\,M_\odot$ and $9.60^{+0.14}_{-0.03}$ km on non-rotating neutron stars with the maximum mass. If we assume the EOSs we used in this paper satisfy the simulations in Bauswein et al. (2013), we can investigate the radius obtained in our work. With $x = 0$, the radii range from 12.15 km/10.41 km to 12.636 km/10.659 km for non-rotating neutron stars with a mass of $1.6\,M_\odot$/maximum mass. Both of them are consistent with the radius constraint.

4 DISCUSSION AND OUTLOOK

We attempt to constrain the EOS of cold, dense nuclear matter from the observations of neutron stars. The slope of symmetry energy L and the incompressibility of symmetric nuclear matter K_0 are crucial to the EOS. A phenomenological approach is used in our work. We base this on the fact that multiple observations of a neutron star will predict the same mass. The observations used in this paper are the maximum glitches and cooling of neutron stars. The MDI interaction based on the Hartree-Fock calculation using the Gogny interaction will be ruled out. When we extend the parameters when x is fixed to zero, we obtain the lower limit of $K_0 = 215\,\mathrm{MeV}$ and $L = 67\,\mathrm{MeV}$ from the observations of 2-solar-mass neutron stars (Demorest et al. 2010; Antoniadis et al. 2013). Moreover, a linear rela-

tionship between L and K_0 can be deduced: $6.173\,\mathrm{MeV} + 0.283K_0 \leq L \leq 7.729\,\mathrm{MeV} + 0.291K_0$. The ranges for the masses of Vela and J1709–4429 are restricted to narrow ranges of $1.45\,M_\odot \sim 1.55\,M_\odot$ and $1.53\,M_\odot \sim 1.62\,M_\odot$ respectively. The constrained EOSs are consistent with the recent observation of GW170817.

We investigate the ranges of masses for glitching pulsars using the method proposed by Pizzochero et al. (2017). In their work, they assume parallel straight vortex lines, pinned only in the crust but threading the whole star. When we refer to the pinning force in the inner crust, only the $^1S_0$ neutrons are taken into consideration. We examine the validity of this assumption. We consider the conventional temperature of the outer core to be $2 \times 10^8\,\mathrm{K}$. It can be deduced that in the inner crust, the critical temperature of $^3P_2$ is below $8 \times 10^7\,\mathrm{K}$, which is smaller than the temperature of the outer core. Moreover, the disconnected vortices are neglected. We claim that the superfluid neutrons will disappear if internal temperature is above the critical temperature of $^3P_2$. There will be a critical mass above which the vortex lines cannot be treated as connected lines. The critical masses of different parameters range from $1.7\,M_\odot$ to $2\,M_\odot$, thus a lower limit of maximum glitch amplitude (around $1 \times 10^{-4}\,\mathrm{rad\,s^{-1}}$) can also be obtained. We also neglect the pinning force in the core due to the $^1S_0$ protons because it is still under debate.

In this work, we only use the observations of Vela and J1709–4429. As listed in Ho et al. (2015); Pizzochero et al. (2017), there are glitch and interior temperature data for J0537–6910, Vela, J1048–5832 (B1046–58), J1341–6220 (B1338–62), J1709–4429 (B1706–44), J1801–2451 (B1757–24), J1803–2137 (B1800–21) and J1826–1334 (B1823–13). However, J0537–6910 cannot be assigned a lower limit due to the lack of ω^*_{pre}. Moreover, B1046–58, B1757–24 and B1823–13 only have an upper limit of T and the uncertainty of B1800–21 is too large. B1338–62 has a maximum $\Delta\Omega$ which equals $1.00 \times 10^{-4}\mathrm{rad\,s^{-1}}$. With some parameters, the masses obtained will exceed the critical mass at which the superfluid neutrons disappear in the center.

In this paper, we fixed $x = 0$ when we use the observations of glitch and cooling to constrain incompressibility and the slope of the symmetry energy. When $x < 0$, the ranges of parameters grow larger, and the ranges constrained by glitch and cooling will also grow larger. We should notice that the radius will be obviously larger with negative x and thus produce a larger tidal deformability parameter. In a future study, we will use GW170817 together with the observations of glitch and cooling of glitching pulsars to constrain the EOS with $x \neq 0$.

The proton superfluid is fixed in our work (1p). The evaluations of M_{I} and M_{II} change severely if we use the 2p proton superfluid model. The values of M_{I} and M_{II} will be larger, and thus both the upper limit and the lower limit of L will be larger. The restricted masses of Vela and J1709–4429 will also be larger. However, the restricted L is not consistent with the observation of GW170817. We will discuss more general EOSs to find out if the 2p model could be totally excluded in future research.

Direct measurements of the masses of glitching pulsars are expected to constrain both the EOS and superfluidity in neutron stars. The degeneration of the EOS and the superfluid model is a serious problem that should be investigated in further work. However, we provide a new method to examine the EOSs. EOSs which lead to masses inconsistent with those obtained from observations of glitches and cooling should be excluded.

Acknowledgements This work was supported by the National Basic Research Program of China (2014CB845800) and the National Natural Science Foundation of China (Grant No. 11573014).

References

Anderson, P. W., & Itoh, N. 1975, Nature, 256, 25
Andersson, N., Glampedakis, K., Ho, W. C. G., & Espinoza, C. M. 2012, Physical Review Letters, 109, 241103
Antonelli, M., & Pizzochero, P. M. 2017, MNRAS, 464, 721
Antoniadis, J., Freire, P. C. C., Wex, N., et al. 2013, Science, 340, 448
Bauswein, A., Baumgarte, T. W., & Janka, H.-T. 2013, Physical Review Letters, 111, 131101
Bauswein, A., Just, O., Janka, H.-T., & Stergioulas, N. 2017, ApJ, 850, L34
Blaizot, J. P. 1980, Phys. Rep., 64, 171
Brockmann, R., & Machleidt, R. 1984, Physics Letters B, 149, 283
Brockmann, R., & Machleidt, R. 1990, Phys. Rev. C, 42, 1965
Brown, G. E., & Osnes, E. 1985, Physics Letters B, 159, 223
Brueckner, K. A., Coon, S. A., & Dabrowski, J. 1968, Physical Review, 168, 1184
Chamel, N. 2012, Phys. Rev. C, 85, 035801
Chamel, N. 2013, Physical Review Letters, 110, 011101
Chamel, N., & Haensel, P. 2006, Phys. Rev. C, 73, 045802
Chen, L.-W., Cai, B.-J., Ko, C. M., et al. 2009a, Phys. Rev. C, 80, 014322
Chen, L.-W., Ko, C. M., & Li, B.-A. 2005, Physical Review Letters, 94, 032701
Chen, L.-W., Ko, C. M., & Li, B.-A. 2007, Phys. Rev. C, 76, 054316

Chen, L.-W., Li, B.-A., Ma, H.-R., & Xu, J. 2009b, in International Workshop on Nuclear Dynamics in Heavy-Ion Reactions and the Symmetry Energy, arXiv:0911.5470
Cooperstein, J. 1985, Nuclear Physics A, 438, 722
Danielewicz, P., & Lee, J. 2014, Nuclear Physics A, 922, 1
Das, C. B., Das Gupta, S., Gale, C., & Li, B.-A. 2003, Phys. Rev. C, 67, 034611
Demorest, P. B., Pennucci, T., Ransom, S. M., Roberts, M. S. E., & Hessels, J. W. T. 2010, Nature, 467, 1081
Douchin, F., & Haensel, P. 2001, A&A, 380, 151
Farine, M., Pearson, J. M., & Tondeur, F. 2001, Nuclear Physics A, 696, 396
Flowers, E., Ruderman, M., & Sutherland, P. 1976, ApJ, 205, 541
Gale, C., Welke, G. M., Prakash, M., Lee, S. J., & Das Gupta, S. 1990, Phys. Rev. C, 41, 1545
Gnedin, O. Y., Yakovlev, D. G., & Potekhin, A. Y. 2001, MNRAS, 324, 725
Hinderer, T., Lackey, B. D., Lang, R. N., & Read, J. S. 2010, Phys. Rev. D, 81, 123016
Ho, W. C. G., Espinoza, C. M., Antonopoulou, D., & Andersson, N. 2015, Science Advances, 1, e1500578 (arXiv:1510.00395)
Hooker, J., Newton, W. G., & Li, B.-A. 2015, MNRAS, 449, 3559
Huber, H., Weber, F., & Weigel, M. K. 1994, Phys. Rev. C, 50, R1287
Jeukenne, J. P., Lejeune, A., & Mahaux, C. 1976, Phys. Rep., 25, 83
Kaminker, A. D., Yakovlev, D. G., & Gnedin, O. Y. 2002, A&A, 383, 1076
Kasen, D., Metzger, B., Barnes, J., Quataert, E., & Ramirez-Ruiz, E. 2017, Nature, 551, 80
Lattimer, J. M. 2012, Annual Review of Nuclear and Particle Science, 62, 485
Lattimer, J. M., & Lim, Y. 2013, ApJ, 771, 51
Lattimer, J. M., & Prakash, M. 2016, Phys. Rep., 621, 127
Levenfish, K. P., & Yakovlev, D. G. 1996, Astronomy Letters, 22, 49
Li, B.-A. 2004, Phys. Rev. C, 69, 064602
Li, B.-A., Chen, L.-W., & Ko, C. M. 2008, Phys. Rep., 464, 113
Link, B., Epstein, R. I., & Lattimer, J. M. 1999, Physical Review Letters, 83, 3362
Lombardo, U., & Schulze, H.-J. 2001, in Lecture Notes in Physics, 578, Physics of Neutron Star Interiors, eds. D. Blaschke, N. K. Glendenning, & A. Sedrakian, 30 (Berlin: Springer Verlag)
Metzger, B. D. 2017, arXiv:1710.05931
Müther, H., Prakash, M., & Ainsworth, T. L. 1987, Physics Letters B, 199, 469
Negele, J. W., & Yazaki, K. 1981, Physical Review Letters, 47, 71
Newton, W. G., Berger, S., & Haskell, B. 2015, MNRAS, 454, 4400
Newton, W. G., Hooker, J., Gearheart, M., et al. 2014, European Physical Journal A, 50, 41
Oertel, M., Hempel, M., Klähn, T., & Typel, S. 2017, Reviews of Modern Physics, 89, 015007
Page, D., Prakash, M., Lattimer, J. M., & Steiner, A. W. 2011, Physical Review Letters, 106, 081101
Pavlov, G. G., Zavlin, V. E., & Sanwal, D. 2002, in Neutron Stars, Pulsars, and Supernova Remnants, ed. W. Becker, H. Lesch, & J. Trümper, 273
Pizzochero, P. M. 2011, ApJ, 743, L20
Pizzochero, P. M., Antonelli, M., Haskell, B., & Seveso, S. 2017, Nature Astronomy, 1, 0134
Pons, J. A., Viganò, D., & Rea, N. 2013, Nature Physics, 9, 431
Prakash, M., Ainsworth, T. L., & Lattimer, J. M. 1988, Physical Review Letters, 61, 2518
Rikovska Stone, J., Miller, J. C., Koncewicz, R., Stevenson, P. D., & Strayer, M. R. 2003, Phys. Rev. C, 68, 034324
Schulze, H.-J., Cugnon, J., Lejeune, A., Baldo, M., & Lombardo, U. 1996, Physics Letters B, 375, 1
Seveso, S., Pizzochero, P. M., Grill, F., & Haskell, B. 2016, MNRAS, 455, 3952
Shlomo, S., Kolomietz, V. M., & Colò, G. 2006, European Physical Journal A, 30, 23
Shternin, P. S., Yakovlev, D. G., Heinke, C. O., Ho, W. C. G., & Patnaude, D. J. 2011, MNRAS, 412, L108
Sjöberg, O. 1974, Nuclear Physics A, 222, 161
Steiner, A. W., & Gandolfi, S. 2012, Physical Review Letters, 108, 081102
Steiner, A. W., Gandolfi, S., Fattoyev, F. J., & Newton, W. G. 2015, Phys. Rev. C, 91, 015804
Steiner, A. W., Lattimer, J. M., & Brown, E. F. 2010, ApJ, 722, 33
Sumiyoshi, K., Toki, H., & Brockmann, R. 1992, Physics Letters B, 276, 393
The LIGO Scientific Collaboration, 2018, arXiv:1805.11579
Trippa, L., Colò, G., & Vigezzi, E. 2008, Phys. Rev. C, 77, 061304
Tsang, M. B., Zhang, Y., Danielewicz, P., et al. 2009, Physical Review Letters, 102, 122701
Wambach, J., Ainsworth, T. L., & Pines, D. 1993, Nuclear Physics A, 555, 128
Watanabe, G., & Pethick, C. J. 2017, Physical Review Letters, 119, 062701
Welke, G. M., Prakash, M., Kuo, T. T. S., Das Gupta, S., & Gale, C. 1988, Phys. Rev. C, 38, 2101
Yakovlev, D. G., Gnedin, O. Y., Kaminker, A. D., & Potekhin, A. Y. 2002, in Neutron Stars, Pulsars, and Supernova Remnants, ed. W. Becker, H. Lesch, & J. Trümper, 287
Yakovlev, D. G., Kaminker, A. D., & Gnedin, O. Y. 2001, A&A, 379, L5
Yakovlev, D. G., Levenfish, K. P., & Shibanov, Y. A. 1999, Physics Uspekhi, 42, 737
Zuo, W., Lejeune, A., Lombardo, U., & Mathiot, J. F. 2002, European Physical Journal A, 14, 469